The magnetic structure of $DyMn_2$

1991 J. Phys.: Condens. Matter 3 727

(http://iopscience.iop.org/0953-8984/3/6/009)

J. Phys.: Condens. Matter 3 (1991) 727–738. Printed in the UK

The magnetic structure of $DyMn_2$

C Ritter†, S H Kilcoyne‡ and R Cywinski‡
† Institut Laue–Langevin, Grenoble, France
‡ J J Thomson Physical Laboratory, University of Reading, Reading RG6 2AF, UK

Received 2 August 1990

Abstract. The evolution with temperature of the magnetic structure of the C15 Laves-phase compound $DyMn_2$ has been studied using powder neutron diffraction and magnetization techniques. The Dy sublattice assumes a spin-canted ferromagnetic structure with 8.8 μ_B per Dy atom. Although all Mn sites within the unit cell are chemically equivalent, only one Mn atom in four is found to possess a magnetic moment (of 1.4 μ_B). These magnetic Mn atoms are located at sites with a strongly polarizing magnetic environment resulting from a near-neighbour configuration of ferromagnetically coupled Dy spins. A spin reorientation is observed at 36 K, and is accompanied by a small thermal expansion anomaly. The Curie temperature of $DyMn_2$ is found to be 45 K.

1. Introduction

It has long been recognized that the rare earth (R)–transition metal (M) intermetallics, based on the formula RM_2 and collectively known as Laves-phase compounds, are ideal model systems with which to examine the interplay between structural, electronic and magnetic properties. In particular, attention has been focused on the mechanisms responsible for 3d-moment formation and subsequent behaviour in these compounds: electronic band widths, Fermi level, local environment and local exchange fields can be varied almost independently by partial or full substitution at either (or both) the R and the M sites.

Compounds for which M = Co, Ni or Fe crystallize with the $MgCu_2$ (C15-type) structure, while those with M = Mn can be divided into two groups: for R = Y, Gd, Tb and Dy the cubic C15 structure is obtained, while for R = Lu, Pr, Nd, Sm, Er and Tm one finds the hexagonal C14 ($MgZn_2$) structure [1–3]. $HoMn_2$, depending upon annealing temperature, can be formed with either the C14 or C15 structure [4]. In the RFe_2 compounds the iron atoms possess well localized magnetic moments, whose magnitude is independent of R, aligned antiparallel to the rare earth moment. The magnetic moment at the cobalt sites in RCo_2 compounds is induced by the exchange field of the magnetic rare earths, while in contrast no nickel moment is observed at all in the corresponding RNi_2 compounds [5–7]. However, neutron diffraction, NMR and thermal expansion measurements show the behaviour of the manganese moment in RMn_2 to be far more interesting.

The magnitude of the Mn moment in RMn_2 compounds appears to be strongly dependent on the Mn–Mn near-neighbour distance. For R = Pr, for which the Mn–Mn distance is 2.76 Å, a maximum Mn moment of just over 3 μ_B has been determined by NMR

0953-8984/91/060727 + 12 $03.50

measurements [8]. Progression from the light to the heavy rare earths reduces the Mn–Mn separation and correspondingly the Mn moment decreases linearly with this separation. When a 'critical' interatomic Mn–Mn spacing of approximately 2.66 Å is reached the Mn moment collapses from its value of 2 μ_B, and for Ho and Er only a relatively small [4] or zero [9] moment is observed in magnetization and NMR measurements.

$DyMn_2$ has a Mn–Mn spacing very close to the critical value. While single-crystal magnetization measurements suggest that this compound has a canted ferrimagnetic structure with 0.6 μ_B per Mn atom [10], NMR clearly shows the presence of two inequivalent Mn sites, one non-magnetic, and the second giving rise to a weak signal consistent with a moment of 2.1 μ_B [11]. This result is particularly intriguing as all 16 Mn sites within the unit cell are chemically equivalent. In order to gain further insight into the nature of the complex magnetic order in $DyMn_2$ we have used high-intensity neutron powder diffractometry, a technique that has already played a crucial role in establishing the long-wavelength helimagnetic structure of YMn_2 [12]. In the case of $DyMn_2$, however, the problem is compounded by the large neutron absorption cross section of Dy. We have been able to circumvent this problem and present the results of our investigation here.

2. Experimental procedure

The stoichiometric Dy–Mn sample was prepared by melting together appropriate quantities of 99.9% pure Dy ingot (Johnson–Matthey) and 99.99% 'puratronic' Mn flakes (Johnson–Matthey) in an argon arc furnace. The resulting ingot was annealed under argon in a tantalum-lined quartz ampoule at a temperature of 800 °C for four days and subsequently cooled rapidly to room temperature. Finally the ingot was crushed to approximately 50 μm powder. AC susceptibility measurements were made using a modified Hartshorn bridge circuit operating at a frequency of 330 Hz, and an applied field of 10 μT. The high-field magnetization measurements were carried out using an Oxford Instruments (UK) vibrating-sample magnetometer in fields of up to 12 T.

The neutron diffraction patterns of the powdered $DyMn_2$ sample were collected using the high-intensity D1B diffractometer at the Institut Laue–Langevin, Grenoble, using an incoming wavelength of 2.52 Å. The multidetector, covering 80° in 2θ-recorded spectra in the d-spacing range of 1.7 Å $< d <$ 9.4 Å. A first spectrum taken with the pure $DyMn_2$ powder sample revealed a strong angle-dependent absorption which rendered a quantitative interpretation of the measured diffraction intensities impossible. However, dilution of the sample with aluminium powder, in the ratio $DyMn_2/Al = 1/10$, proved to be an adequate means of overcoming this problem; contamination of the resulting spectra due to Al reflections was not too severe. A transmission measurement in the direct beam was performed to evaluate the absorption coefficient of the $DyMn_2/Al$ mixture.

A standard ILL 'orange' cryostat was used to vary the sample temperature in the range 2 K to 100 K. The spectrum at the lowest temperature was measured for 30 minutes, and a temperature scan over the range 20 K $< T <$ 100 K was performed with a heating rate of 16 min K^{-1}, with a new spectrum being started every 15 minutes.

3. Results and discussion

3.1. AC susceptibility and magnetization

The temperature dependence of the real and imaginary components of the AC susceptibility, χ and χ' respectively, of the polycrystalline $DyMn_2$ sample are shown

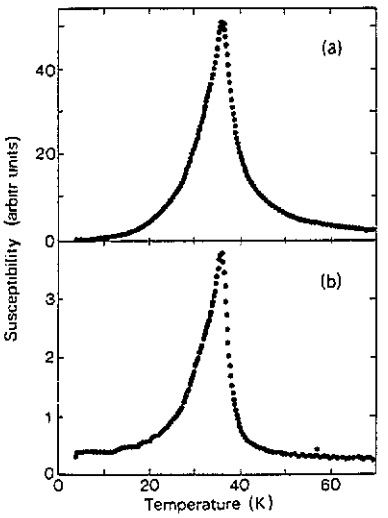

Figure 1. (*a*) Real and (*b*) imaginary components of the AC susceptibility of $DyMn_2$ measured at 330 Hz in a field of 10 μT.

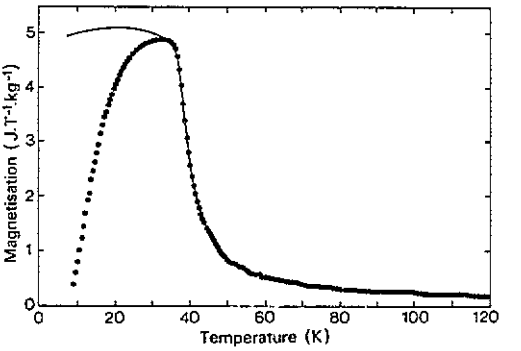

Figure 2. Low-field (20 mT) DC magnetization of $DyMn_2$ measured in the zero-field-cooled (circles) and field-cooled (full curve) states.

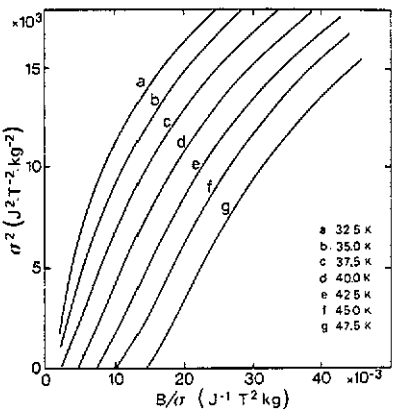

Figure 3. Arrott plots (σ^2 versus B/σ) for the $DyMn_2$ sample at temperatures between 32.5 K and 47.5 K. Note that 45 K is the highest temperature at which a tangent to the isotherm can intercept the σ^2-ions.

in figure 1. Both show a sharp and slightly asymmetric peak at 36 K. Low-field DC magnetization measurements (made in a field of 20 mT) show a similar peak at 36 K, but here the asymmetry in the temperature dependence is more pronounced (figure 2). Although it is apparent that there is an important magnetic transition at 36 K, detailed analysis of the magnetic isotherms, at temperatures between 35 K and 50 K and obtained in fields of up to 6 T, show the Curie temperature to be somewhat higher than this value: although Arrott plots of σ^2 versus B/σ [13] constructed from the isotherms (suitably corrected for demagnetization effects) show marked deviations from Arrott's mean-field calculations at low magnetic fields, extrapolation of the isotherms at higher values of B suggest a Curie point close to 45 K, as can be seen in figure 3.

At 4 K, saturation of the magnetization of the $DyMn_2$ sample is not fully attained. However, extrapolation to $1/B = 0$ yields a saturation magnetization of 175 J T^{-1} kg^{-1}.

This corresponds to a magnetic moment per formula unit of 8.5 μ_B, in reasonable agreement with the single-crystal magnetization measurements reported by Makihara *et al* [10] where a value of 8.9 μ_B FU^{-1} was found. Above T_N a plot of inverse susceptibility against temperature deviates from linearity up to temperatures of approximately 250 K, perhaps indicating magnetic short-range order. Above this temperature the effective paramagnetic moment of $DyMn_2$, determined from the Curie constant, takes a value of 10.6 μ_B FU^{-1} and the paramagnetic Curie temperature, θ_p, is 35 K (cf [10] where 11.2 μ_B FU^{-1} and 35 K respectively, are reported). P_{eff} is thus close to the free-ion value for Dy.

3.2. Neutron diffraction

Figure 4 shows a three dimensional thermogram of the temperature-dependent diffraction pattern of the $DyMn_2$/Al mixture. In addition to the five nuclear Bragg reflections, arising from the C15 structure, falling within the 2θ range covered by the multidetector, several new peaks appear on cooling the sample. These additional antiferromagnetic peaks were first indexed according to a doubling of the cubic nuclear cell in all three lattice directions. As well as the antiferromagnetic Bragg peaks there is a clear indication of the evolution of a ferromagnetic contribution at the nuclear Bragg positions at low temperatures. Figure 5(*a*) displays the integrated intensity of the (nuclear) 111 peak as a function of temperature. The magnetic contribution is seen to disappear at 45 K, in agreement with the Curie point determined from the Arrott plots of figure 3. Figure 5(*b*) shows the behaviour of the low-angle antiferromagnetic peak indexed as (111) in the doubled cell. After decreasing continuously between 20 K and 30 K the integrated intensity of this peak recovers suddenly showing a maximum at 37 K before decreasing to zero at 45 K. We can already conclude that the magnetic structure of $DyMn_2$ has both ferro- and antiferromagnetic components at low temperatures, and, moreover, that a pronounced spin reorientation takes place in the temperature range 30 K to 40 K. The temperature at which this spin reorientation takes place is in close agreement with that of the sharp peak in the AC susceptibility and low-DC-field magnetization data.

A sequential refinement of the nuclear cell volume as a function of temperature has provided the data shown in figure 6. For $DyMn_2$ there is no evidence of the massive magnetovolume effects previously observed in warming $TbMn_2$, YMn_2 and $GdMn_2$ through their ordering temperatures. For these latter compounds a collapse in the volume of the unit cell of 1.8%, 4.8% and 0.5% respectively, is observed at the magnetic ordering temperature. However, marked departures from normal thermal expansion behaviour in the temperature range 31 K to 50 K are clearly seen. Above the magnetic ordering temperature the nuclear structure was refined using a modified Rietveld program [14], confirming the C15 $MgCu_2$ structure (space group $Fd3m$), with a resulting R-factor of $R_{wp} = 5.1\%$.

The low-temperature magnetic structure is characterized by the existence of additional magnetic peaks which, when indexed on the doubled nuclear cell, have all odd indices (111, 311, 331 . . .), thereby suggesting a magnetic structure similar to that of MnO, in which spins in each 111-plane are parallel to each other but antiparallel to neighbouring 111-planes. Applying this scheme to the $MgCu_2$ structure of the $DyMn_2$ compound one sees that the Dy atoms form two sublattices shifted by $\frac{1}{4}, \frac{1}{4}, \frac{1}{4}$ relative to each other. A simulation of the intensity differences between the spectra collected at 2 K and 50 K supported the model of two Dy sublattices each with the MnO-type

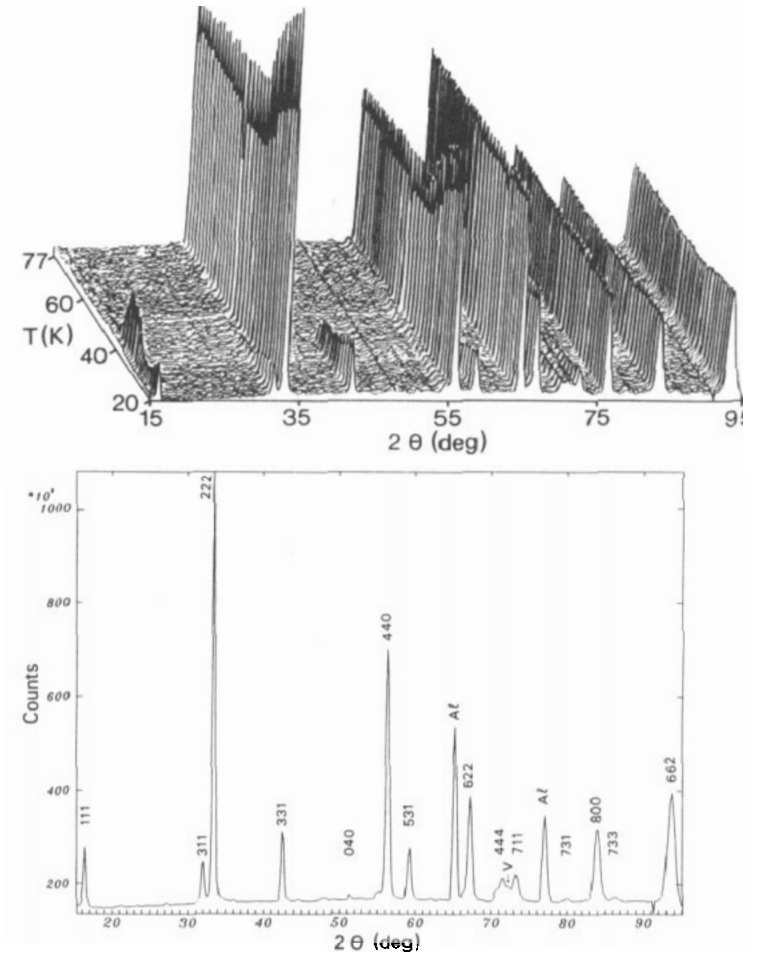

Figure 4. Evolution of the neutron diffraction spectra (λ = 2.52 Å) between 20 K and 77 K. Antiferro- and ferromagnetic components can be seen at low temperatures. Below: indexing of the diffraction peaks at low T using the double cubic unit cell.

antiferromagnetic arrangement of Dy spins. However, in order to account for the magnetic contribution to the nuclear Bragg peaks an additional ferromagnetic component had to be assumed. The resulting spin structure lowers the originally cubic symmetry: as shown by Bertaut [15], the classical example of MnO itself has to be described in the monoclinic Shubnikov groups $P2/m$ (spins along $[1\bar{1}0]$) or $P2'/m'$ (spins along $[11\bar{2}]$). The existence of an additional ferromagnetic spin component breaks the symmetry completely.

To avoid working with the excessively large number of atoms within a magnetic unit cell based on a doubling of the nuclear cell in all three directions an orthorhombic cell was chosen with $a = \frac{1}{2}a_i + \frac{1}{2}a_j$, $b = -a_i + a_j$, and $c = 2a_k$, where a_i, a_j and a_k define the original cube edges. The even smaller primitive cell with $a = \frac{1}{2}a_i + \frac{1}{2}a_j$, $b = -a_i + a_j$ and $c = \frac{1}{2}a_i - \frac{1}{2}a_j + a_k$ and $\beta = \gamma = 90°$, $\alpha = 54.74°$ was rejected for the sake of clarity. Figure

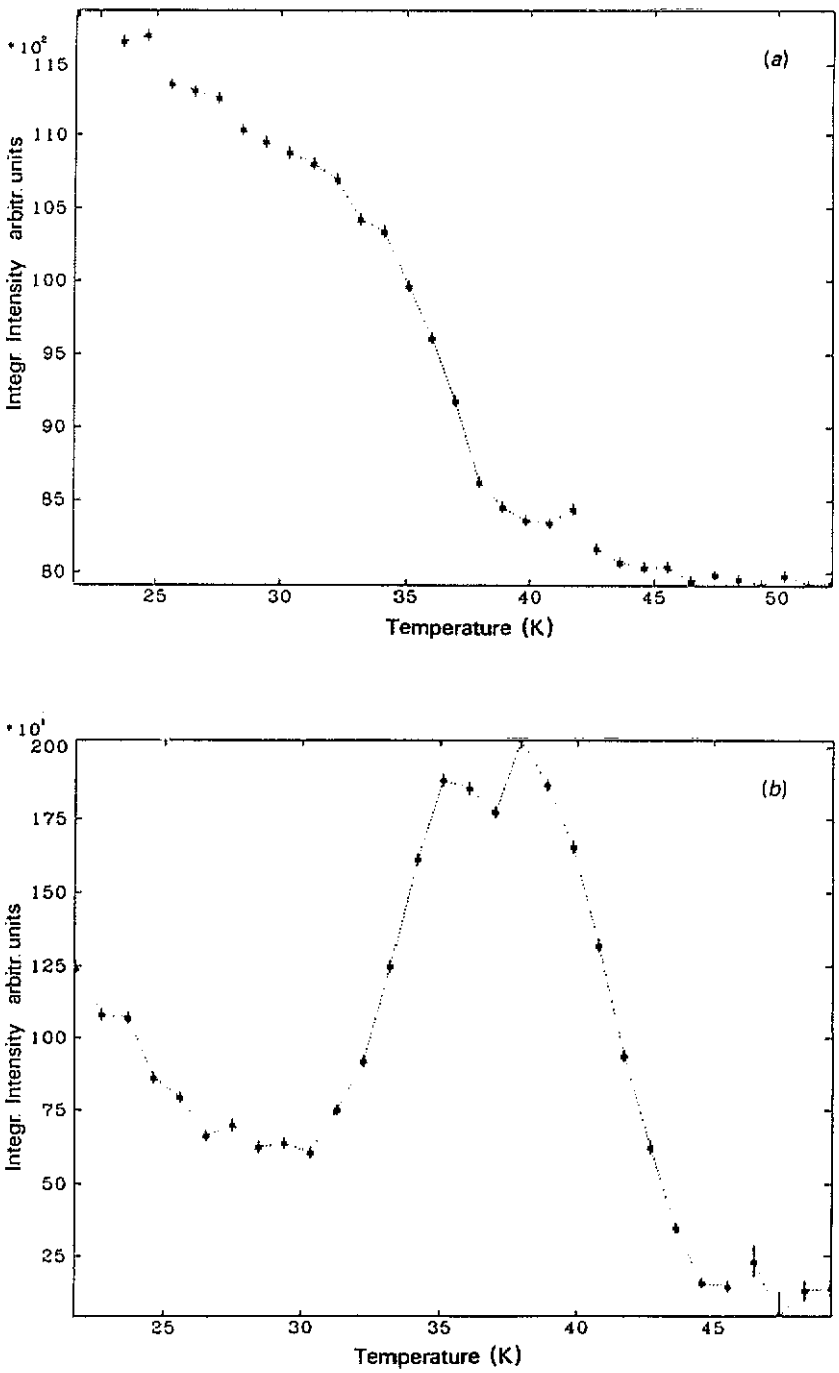

Figure 5. (*a*) Integrated intensity of the nuclear 111-peak between 20 K and 53 K. The magnetic contribution disappears at about 45 K. (*b*) Integrated intensity of the magnetic 111-peak between 20 K and 50 K. A spin reorientation sets in at about 30 K; the peak disappears at about 45 K.

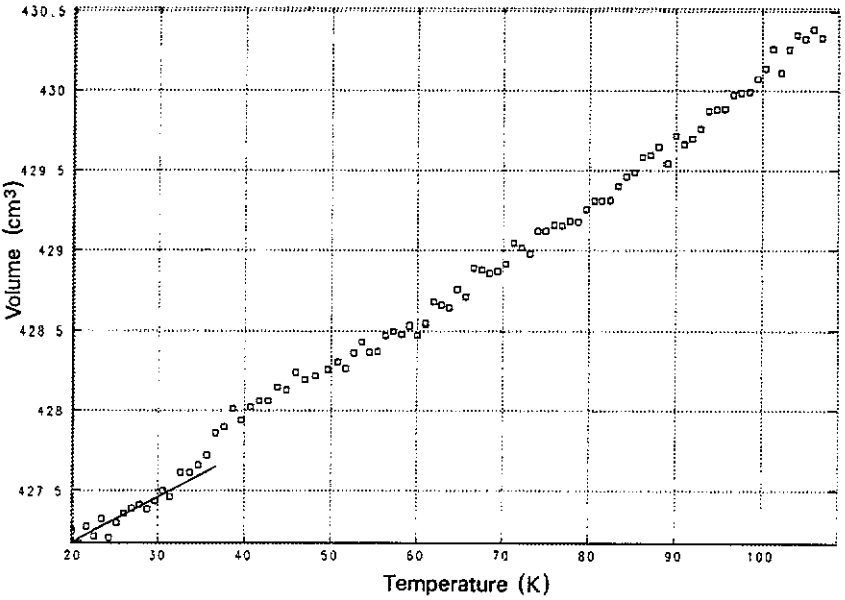

Figure 6. Evolution of the unit cell volume of $DyMn_2$ between 20 K and 110 K. The small anomaly in the thermal expansion seen at about 30 K is related to a spin reorientation of the Dy spins.

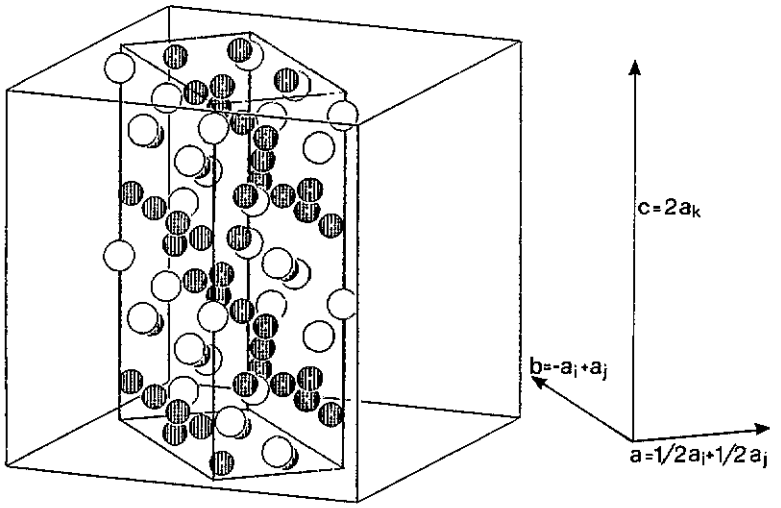

Figure 7. Orthorhombic unit cell used for the Rietveld refinement of the low-T magnetic structure of $DyMn_2$. a_i, a_j and a_k are the lattice dimensions of the original cubic cell.

7 displays the new unit cell containing 16 Dy and 32 Mn atoms. Using this starting model a Rietveld refinement of the magnetic structure at 2 K was undertaken using a modified version of the BNL programs using a locally modified version of the original Rietveld program [16]. Form factors for Dy^{3+} and Mn^{2+} were calculated using the tables published

Table 1. Results of the Rietveld refinement for $DyMn_2$ at 2 K. No magnetic moment on the Mn site is assumed.

$\mu_{Dy\,A}$ (μ_B)	8.88 (85)
K_x	6.47 (72)
K_y	−2.66 (24)
K_z	5.47 (44)
a	5.3148 (3)
b	10.6537 (9)
c	15.0393 (14)
R_{Bragg}	11.0
R_p	15.0
R_{wp}	15.0
R_{Nuc}	6.6
R_{Mag}	17.3

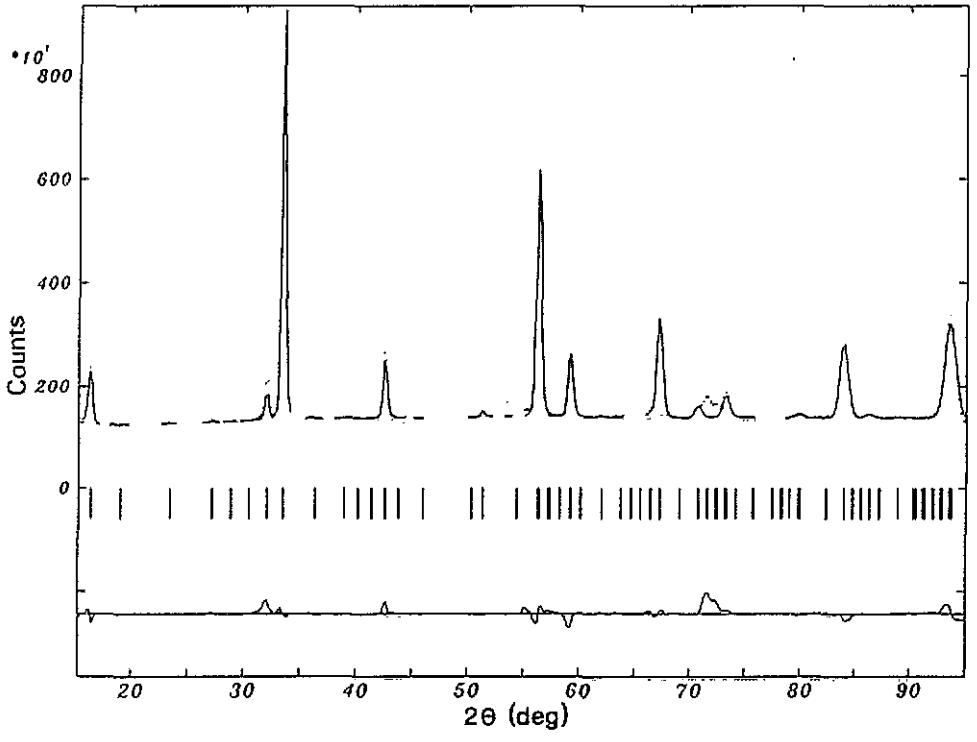

Figure 8. Observed, calculated and difference powder neutron diffraction profiles of $DyMn_2$ assuming a magnetic moment only on the rare earth site.

by Brown [17]. The positional parameters of the atoms were kept fixed in the refinement. As additional degrees of freedom, the program was allowed to vary the orthorhombic lattice parameters away from the ideal values calculated for the original cubic unit cell. Defining the magnetic spin direction of the Dy moments of one cubic 111-plane as K_x, K_y, K_z those of the neighbouring 111-planes of the same sublattice were restricted to the direction K_x, $-K_y$, $-K_z$. Table 1 contains the results of the Rietveld refinement, and

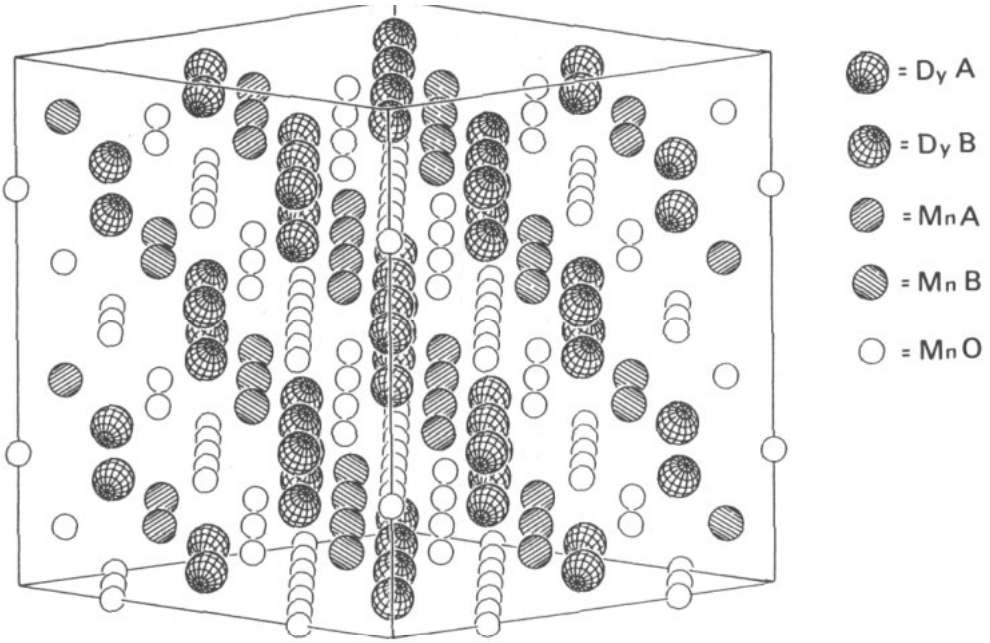

Figure 9. The magnetic structure of $DyMn_2$: Mn A atoms interposed between 111-planes of Dy A spins, Mn B atoms interposed between 111-planes of Dy B spins, Mn O atoms sitting on sites with magnetic inversion symmetry.

figure 8 shows a plot of the measured, calculated and difference spectra. At this stage of refinement no moment was assumed at any Mn site. Attempts at introducing a magnetic moment at these sites, oriented antiparallel to the ferromagnetic component of the Dy sublattice, proved unsuccessful.

Figure 9 shows how the magnetic structure of the Dy sublattice breaks the symmetry between the Mn sites. Labelling the two spin orientations of the Dy moments as A and B, the originally equivalent Mn sites now split into three different types. For three out of four Mn sites the magnetic environment due to the Dy spins is symmetric with an equal number of equidistant A- and B-type spins. The remaining 25% of the Mn sites, however, are interposed between 111-planes of Dy spins belonging to the two Dy sublattices and which have the same spin orientation. Successive attempts to refine a Mn moment clearly revealed that only those Mn atoms at the latter sites, i.e. those with a strongly polarizing magnetic surrounding, possess a magnetic moment. We find from the profile refinement that the Mn atoms sandwiched between the ferromagnetic Dy layers align closely antiparallel to the Dy spins, and therefore also antiparallel to the Mn spins of the next sandwiched Mn layer. Table 2 and figure 10 show the results of the final fit. It can be seen that the introduction of the magnetic moment on every fourth Mn site improves the refinement significantly. The value for the Dy moment, $\mu_{Dy} = 8.83\ (17)\ \mu_B$ is in good agreement with the saturation moment of $8.9\ \mu_B\,FU^{-1}$ as determined by Makihara *et al* [10] and with our own value of $8.5\ \mu_B\,FU^{-1}$. Agreement with the latter is further improved when the antiferromagnetically coupled Mn moment of $1.4\ \mu_B$ found here for 25% of the Mn sites is included in the calculation of the net saturation moment per formula unit. The value of $\mu_{Mn} = 1.4\ \mu_B$ also compares reasonably well with the

Table 2. As table 1 but including a moment on every fourth Mn site (see text).

$\mu_{Dy\,A}$ (μ_B)	8.83 (73)
K_x	6.47 (63)
K_y	−2.40 (30)
K_z	5.51 (40)
$\mu_{Mn\,A}$ (μ_B)	1.41 (18)
K_x	—
K_y	0.84 (43)
K_z	−1.12 (28)
a	5.3174 (3)
b	10.6579 (6)
c	15.0270 (8)
R_{Bragg}	7.3
R_p	12.3
R_{wp}	12.9
R_{Nuc}	6.3
R_{Mag}	8.6

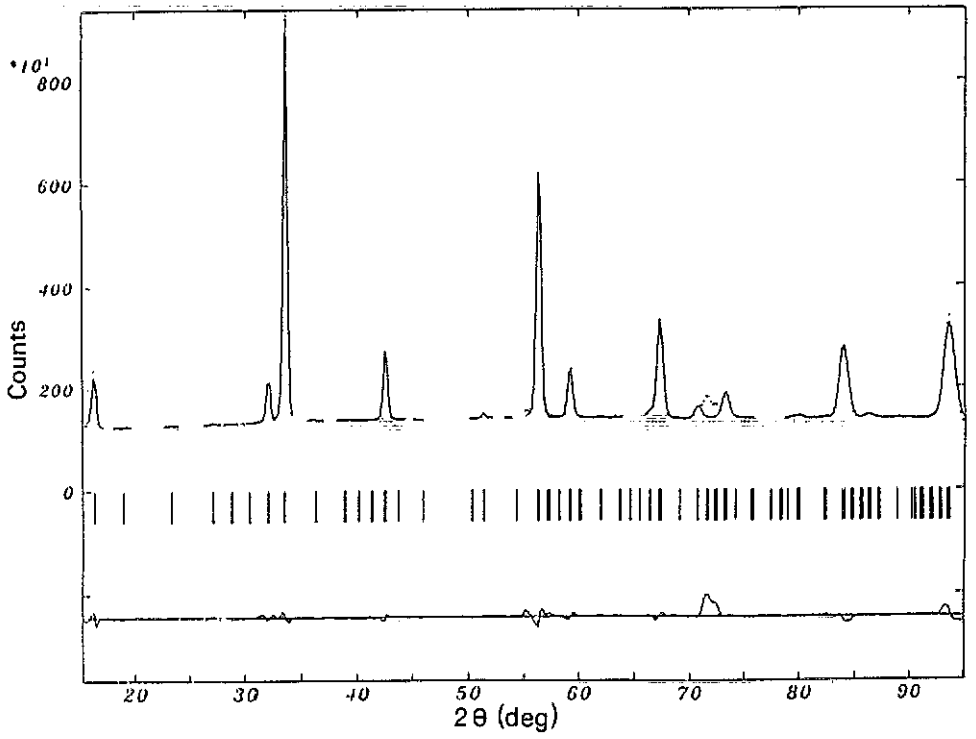

Figure 10. The final observed, calculated and difference powder neutron diffraction profiles at 2 K assuming an additional moment on every fourth Mn site.

moment of $2\mu_B$ suggested for a fraction of the Mn sites in $DyMn_2$ by the NMR results of Yoshimura *et al* [11].

Using the known magnetic spin structure at 2 K, the evolution with temperature was analysed by successive Rietveld refinement of the data taken in the 20 K to 50 K

Table 3. Evolution of the magnetic moments in $DyMn_2$. A spin reorientation of the Dy moments sets in at about 30 K; the manganese magnetic moment disappears at the same temperature as the Dy moment. Dy B and Mn B behave as K_x, $-K_y$, $-K_z$ relative to Dy A and Mn A.

T (K)	$\mu_{Dy\,A}$ (μ_B)	K_x	K_y	K_z	$\mu_{Mn\,A}$(μ_B)
2	8.82 (73)	6.46 (62)	−2.40 (30)	5.51 (40)	−1.41 (18)
20	8.73 (36)	6.78 (33)	−2.16 (13)	5.07 (15)	−1.33 (13)
22	8.44 (34)	6.57 (33)	−2.20 (12)	4.83 (13)	−1.36 (12)
24	8.32 (36)	6.52 (35)	−2.39 (14)	4.58 (14)	−1.39 (14)
27	7.77 (34)	6.23 (34)	−1.97 (14)	4.21 (13)	−1.28 (14)
29	7.12 (33)	5.67 (33)	−1.28 (14)	4.11 (12)	−0.92 (14)
31	6.80 (34)	5.51 (35)	0.14 (20)	4.00 (14)	−0.96 (16)
33	5.70 (31)	4.37 (33)	0.97 (32)	3.53 (18)	−0.87 (16)
35	5.03 (34)	3.24 (43)	1.68 (60)	3.46 (35)	−1.17 (20)
37	3.57 (36)	1.21 (87)	1.41 (62)	3.05 (36)	−0.90 (20)
39	3.21 (39)	1.85 (59)	1.14 (83)	2.36 (47)	−0.82 (28)
41	2.77 (48)	2.34 (53)	−0.27 (42)	1.45 (18)	−0.57 (37)

temperature range. As the counting statistics of the spectra taken with increasing temperature was not as good as that for the 2 K spectrum, the Mn spins were restricted to lie in the $\pm z$ direction. Table 3 provides the results of the refinements between 20 K and 41 K, in addition to those obtained at 2 K. The disappearance of an ordered moment at the Mn site coincides with the disordering of the Dy moments at 45 K. The change in intensity of the antiferromagnetic peaks starting at 30 K can clearly be associated with a reorientation of the rare earth moments, as can the anomalous thermal expansion of the $DyMn_2$ cell between 30 K and 50 K. In contrast to the massive collapse of the cell volume of YMn_2 at T_N, this anomaly cannot be related to the collapse of the Mn moment itself: in $DyMn_2$ the ordered Mn moment decreases continuously as a function of temperature rather than exhibiting the first-order collapse to the non-magnetic state seen in YMn_2.

4. Conclusions

As discussed in section 1, it has previously been shown that there is a marked correlation between the magnitude, and indeed the presence, of a magnetic moment at the Mn site in the RMn_2 Laves-phase compounds, and the Mn–Mn interatomic distance. Using the criteria proposed by Shiga [18], $DyMn_2$ lies at the borderline between those compounds possessing a Mn moment and those with a negligible or zero moment. One might therefore expect the Mn moment in $DyMn_2$ to be highly unstable, and such an instability is further suggested by NMR measurements [11] which show only some of the structurally equivalent Mn atoms to possess a moment. Through our neutron diffraction measurements, this result can now be seen as a consequence of the magnetic spin structure of the Dy sublattice: the spin-canted structure of the Dy gives rise to ferromagnetically coupled double 111-layers between which 25% of the Mn atoms are sandwiched in a strongly polarizing magnetic environment. The Mn moments are sufficiently close to the point of localization that the strong exchange field from the Dy spins induces a localized moment of 1.4 μ_B, in a fashion analogous to that observed at the Co sites in isostructural

RCo_2 compounds [6]. The remaining Mn atoms reside on sites with magnetic inversion symmetry and carry no moment. The dependence of the manganese moment on magnetic environment as well as on the width of the 3d band, determined by Mn–Mn separation, introduces an extra degree of complexity to the model proposed by Shiga [18].

Acknowledgments

The authors would like to thank Mr A Perkin of Reading University for his technical support. Financial support from the Neutron Beam Research Committee of the SERC is also gratefully acknowledged.

References

[1] Wernick J H and Geller S 1960 *Trans. AIME* **218** 866
[2] Nassau K, Cherry L V and Wallace W E 1960 *J. Phys. Chem. Solids* **16** 123
[3] Wernick J H and Haszko S E 1961 *J. Phys. Chem. Solids* **18** 207
[4] Hardmann K, Rhyne J J, Malik S and Wallace W E 1982 *J. Appl. Phys.* **53** 1944
[5] Buschow K H J and van Stapele R P 1970 *J. Appl. Phys.* **41** 4066
[6] Moon R M, Koehler W C and Farrell J 1965 *J. Appl. Phys.* **36** 978
[7] Givord D, Givord F, Gignoux D, Koehler W C and Moon R M 1976 *J. Phys. Chem. Solids* **37** 567
[8] Yoshimura K and Nakamura Y 1984 *J. Phys. Soc. Japan* **53** 3611
[9] Shimizu K, Dhar S K, Vijayaraghavan R and Malik S K 1981 *J. Phys. Soc. Japan* **50** 1200
[10] Makihara Y, Andoh Y, Hashimoto Y, Fujii H, Hasuo M and Okamoto T 1983 *J. Phys. Soc. Japan* **52** 629
[11] Yoshimura K, Shiga M and Nakamura Y 1986 *J. Phys. Soc. Japan* **55** 3585
[12] Ballou R, Deportes J, Lemaire R, Nakamura Y and Ouladdiaf B 1987 *J. Magn. Magn. Mater.* **70** 129
[13] Arrott A 1957 *Phys. Rev.* **108** 1394
[14] Rodriguez J, Anne M and Pannetier J 1987 *Institut Laue–Langevin Report* 87RO14T
[15] Bertaut E F 1972 *Ann. Phys., Lpz.* **7** 203
[16] Rietveld H M 1969 *J. Appl. Cryst.* **2** 65
[17] Brown P J 1991 *International Tables for Crystallography* vol C (Dordrecht: Reidel) to be published
[18] Shiga M 1988 *Physica* B **149** 293